Communication

Multi-Fused S,N-Heterocyclic Compounds for Targeting α-Synuclein Aggregates

Chao Zheng , Jeffrey Stehouwer , Goverdhan Reddy Ummenthala , Yogeshkumar Munot , Neil Vasdev *

Posted Date: 30 May 2025

doi: 10.20944/preprints202505.2503.v1

Keywords: α-Synuclein, PET; Parkinson's disease; structure-activity relationships

 doi:10.20944/preprints202505.2503.v1

Communication

Multi-Fused S,N-Heterocyclic Compounds for Targeting α-Synuclein Aggregates

Chao Zheng [1], Jeffrey S. Stehouwer [2], Goverdhan Reddy Ummenthala [3], Yogeshkumar S. Munot [3] and Neil Vasdev [1,*]

[1] MedChem Imaging, Inc. Boston, MA, 02210, USA.

[2] Department of Radiology, University of Pittsburgh, Pittsburgh, PA 15213, USA.

[3] Laxai Life Sciences, Hyderabad, Telangana, 500078, India.

* Correspondence: neil@medchemimaging.com

Abstract: The development of positron emission tomography (PET) tracers targeting α-synuclein (α-syn) aggregates is critical for the early diagnosis, differential classification, and therapeutic monitoring of synucleinopathies such as Parkinson's disease (PD), dementia with Lewy bodies (DLB), and multiple system atrophy. Despite recent advances, challenges including the low abundance of α-syn aggregates (10–50× lower than amyloid-beta (Aβ) or Tau), structural heterogeneity (e.g., flat fibrils in PD vs. cylindrical forms in DLB), co-pathology with Aβ/Tau, and poor metabolic stability have hindered PET tracer development for this target. To optimize our previously reported pyridothiophene-based radiotracer, [^{18}F]asyn-44, we present the synthesis and evaluation of novel S,N-heterocyclic scaffold derivatives for α-syn. A library of 49 compounds was synthesized, with eight potent derivatives (LMD-006, LMD-022, LMD-029, LMD-044, LMD-045, LMD-046, LMD-051, and LMD-052) demonstrating equilibrium inhibition constants (K_i) of 6–16 nM in PD brain homogenates, all of which are amenable for radiolabeling with fluorine-18. This work advances the molecular toolkit for synucleinopathies and provides a roadmap for overcoming barriers in PET tracer development, with lead compounds that can be considered for biomarker-guided clinical trials and targeted therapies.

Keywords: α-Synuclein; PET; Parkinson's disease; structure-activity relationships

1. Introduction

Synucleinopathies, including Parkinson's disease (PD), dementia with Lewy bodies (DLB), and multiple system atrophy (MSA), are defined by the pathological accumulation of α-synuclein (α-syn) aggregates in neurons or glia [1-3]. These aggregates propagate in a prion-like manner, correlating with neurodegeneration and clinical progression [4]. Current diagnosis relies on nonspecific motor or cognitive symptoms, often delaying intervention until irreversible neuronal loss occurs [5]. The pathological progression of synucleinopathies, is strongly associated with the accumulation of aggregated α-syn, spurring the development of α-syn-targeted positron emission tomography (PET) radiotracers as non-invasive biomarkers for early diagnosis, differential classification (e.g., distinguishing PD from MSA), and therapeutic monitoring. Such imaging agents would not only facilitate target engagement studies for α-syn-directed therapies but also enhance patient stratification in clinical trials [2, 6-10] (Fig.1). The recent United States Food and Drug Administration (FDA) endorsement of α-syn seed amplification assays (αSyn-SAA) underscores the growing need for complementary in vivo imaging modalities to validate and extend biochemical diagnostic approaches, supporting a more comprehensive and precise management strategy for synucleinopathies [11].

Developing α-syn PET tracers faces formidable challenges: (1) α-syn aggregates occur at 10–50 times lower concentrations than amyloid-beta (Aβ) or tau, necessitating tracers with low- to sub-nanomolar affinity; (2) structural similarities between β-sheet-rich amyloid proteins demand high

 doi:10.20944/preprints202505.2503.v1

selectivity to avoid off-target binding; (3) post-translational modifications (e.g., phosphorylation at S129) and fibril polymorphism (e.g., flat vs. twisted conformations) complicate universal ligand design; and (4) intracellular α-syn inclusions require tracers to cross the blood-brain barrier (BBB) and cell membranes while resisting rapid metabolism [7, 12-17]. Despite extensive efforts by academic laboratories and pharmaceutical companies, no α-syn tracer has achieved clinical validation for PD. PET radiopharmaceuticals (**Figure 1**) such as [^{18}F]F0502B (binds α-syn fibrils with K_d = 10.97 nM) [18], [^{18}F]ACI-12589 (selectively detects MSA pathology) [14], and [^{18}F]C05-05 (binds DLB tissue with IC_{50} = 1.5 nM) have shown promise for imaging α-syn [19]. However, these compounds are limited by either insufficient selectivity or poor metabolic stability. More recently, the development of [^{11}C]M503-1619, a tracer with high affinity for α-syn fibrils (K_i = 6.5 nM) and strong binding in PD brain tissue (K_d = 1.5 nM), has emerged as a promising radioligand for imaging α-syn pathology. Nonetheless, its rapid metabolic degradation may hinder its utility in long-duration scans and complicates quantitative imaging analyses using blood-input-based pharmacokinetic modeling [20].

Our recent efforts to develop PET radiotracers for α-syn have focused on diverse scaffolds such as phenothiazines, diphenylpyrazoles, and benzothiazoles. Among these, pyridothiophenes, exemplified by [^{18}F]asyn-44, emerged as particularly promising due to their modular synthetic accessibility and the high binding affinity of [^{3}H]asyn-44 (K_d = 1.85 nM) in post-mortem PD brain tissue, with minimal off-target interaction with amyloid-β (Aβ). Guided by cryo-EM structural insights into α-syn binding pockets, we previously synthesized a series of 47 derivatives to explore structure–activity relationships (SAR), evaluated their binding in PD brain homogenates, and performed preliminary in vivo PET imaging with [^{18}F]asyn-44 [16]. These studies reinforced the potential of the pyridothiophene scaffold while also identifying radiometabolic instability in rodent brain as a potential limitation.

Herein, we report the synthesis and evaluation of a novel series of S,N-heterocyclic scaffold derivatives based on [^{18}F]asyn-44. A focused library of 49 compounds, with the goal of being amenable for radiolabeling for PET, was synthesized, from which eight derivatives, showed high affinity for α-syn, with equilibrium inhibition constants (K_i) ranging from 6 to 16 nM in PD brain homogenates. The most promising compound was evaluated for metabolic stability in human liver microsome assays as a potential substrate for efflux transporters, to confirm pharmacokinetic properties suitable for in vivo PET imaging applications.

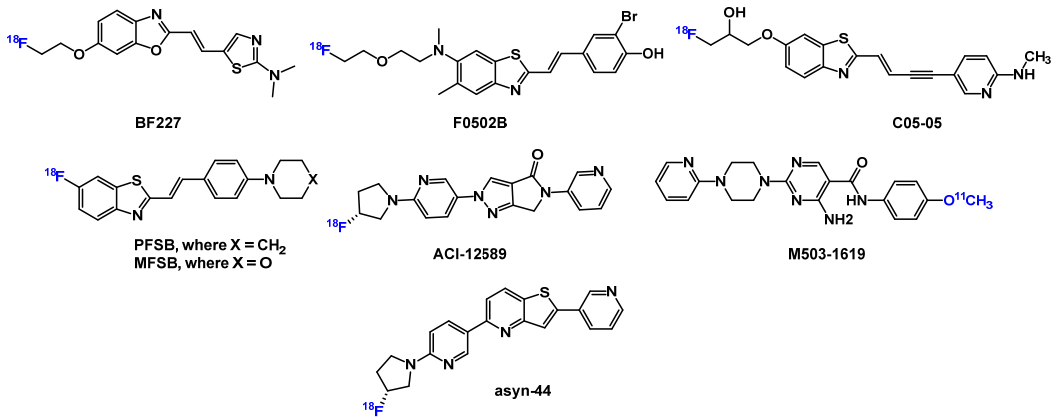

Figure 1. Selected PET tracers for imaging α-syn.

2. Materials and Methods

General

All ligands for this study were provided by MedChem Imaging, Inc. (Boston, USA) with >95% purity. [^{3}H]Asyn-44 (1.5 GBq/μmol, 36 MBq/mL) was labelled with tritium gas from the respective

 doi:10.20944/preprints202505.2503.v1

dibromo precursor by Novandi Chemistry AB (Södertälje, Sweden) [16]. All other chemicals and reagents were obtained from commercial vendors and were used as received without further purification. Thin layer chromatography (TLC) was performed using TLC silica gel 60 F25425 (Merck) plates for monitoring reactions, and the spots were visualized under UV light (254 nm). Flash chromatography purifications were conducted on a Biotage Isolera One system (Uppsala, Sweden) and Combi-flash Nextgen 100 (Teledyne ISCO, Lincoln, USA). ^{1}H-NMR spectra were recorded on a Bruker NEO-400 spectrometer (Bruker, Switzerland.) with chemical shifts (δ) reported in parts per million (ppm) relative to the deuterated solvent as an internal reference. Mass spectra (*m*/*z*) were acquired on a UPLC-MS Aquity SQD2 (Waters Corporation, MA, U.S.A.) with positive electrospray ionization (ESI+), and high-performance liquid chromatography was performed using a Waters 2695 Alliance (Waters Corporation, MA, U.S.A.).

Postmortem Tissues

Anterior cingulate cortex tissue from a Parkinson's disease (PD) case was generously provided by Dr. Thomas Beach at the Banner Sun Health Research Institute in Arizona, USA. This sample showed abundant *α*-synuclein pathology without evidence of aggregated amyloid or TDP-43 inclusions. Preparation of the frozen blocks for binding assays followed previously established protocols [16, 21].

In Vitro Competition (K_i) Assays

The equilibrium inhibition constants (K_i) for the unlabeled compounds were measured against [^{3}H]asyn-44 using our previously reported procedure [16]. For these assays, frozen aliquots of homogenized human brain tissue (stored at −80°C) were used. Homogenates were prepared at 10 mg/mL in phosphate-buffered saline, then diluted with 50 mM Tris buffer (pH 7.0) to a working concentration of 1 mg/mL.

Unlabeled competitor compounds were initially dissolved in DMSO at 400 μM, then diluted with Tris buffer to 20 μM, resulting in a 5% DMSO concentration. A serial dilution series (ranging from 6 μM to 4 nM) was prepared in the same 5% DMSO/Tris buffer solution to maintain consistent solvent conditions throughout the assay.

To perform the binding assay, 50 μL of the appropriately diluted competitor solution was mixed with 50 μL of [^{3}H]asyn-44 (1 nM final concentration), and 800 μL of Tris buffer containing 20% ethanol and 0.1% bovine serum albumin (BSA). Then, 100 μL of the 1 mg/mL brain homogenate was added, bringing the final tissue concentration to 100 μg/mL. The reaction mixtures were incubated at room temperature for 60 minutes before filtration through Whatman GF/B glass fiber filters using a Brandel M-24R cell harvester (Gaithersburg, MD, USA). Filters were washed three times with 3 mL of Tris buffer containing 20% ethanol and 0.1% BSA.

After washing, retained radioactivity was measured using CytoScint-ES scintillation fluid following thorough vortexing. Specific binding was calculated by correcting for nonspecific binding (as described later), and the amount of bound radioligand was derived from the filter-associated radioactivity and the molar activity of the tritiated compound.

Two Point Screening Assays

Screening assays for the test compounds were performed at two concentrations—30 nM and 300 nM—using unlabeled competitors in human PD brain homogenates against [^{3}H]asyn-44 as previously described [16]. To establish assay baselines, 0% inhibition was defined by the total binding observed in the absence of any unlabeled competitor, while 100% inhibition (representing nonspecific binding) was defined by the binding measured in the presence of 1 μM of the unlabeled radioligand. The % inhibition of the radioligand by the test compound at 30 or 300 nM was defined by the number of counts specifically bound at 30 or 300 nM divided by the difference of counts at 0% inhibition

 doi:10.20944/preprints202505.2503.v1

minus the counts at 100% inhibition multiplied by 100. Each assay was conducted in triplicate for both concentrations to ensure reproducibility and statistical reliability.

Metabolic Stability in Human Liver Microsomes

Metabolic stability assays were conducted using pooled human liver microsomes (HLMs) to evaluate the rate of in vitro metabolic degradation of the test compound. Incubations were carried out in duplicate (n = 2) at a final compound concentration of 1 μM. The protein concentration of the microsomal suspension was adjusted to 0.5 mg/mL using phosphate buffer (100 mM, pH 7.4). Reactions were initiated by the addition of NADPH (final concentration 1 mM) and incubated at 37°C. Aliquots were taken at four time points: 0, 5, 15, and 30 minutes. Each reaction was quenched with ice-cold acetonitrile containing internal standard, followed by centrifugation to pellet proteins. Supernatants were analyzed using a validated LC-MS/MS method to determine the concentration of the parent compound at each time point. Verapamil was used as a reference compound to verify assay performance. Metabolic stability was assessed by calculating the percentage of the parent compound remaining at each time point. The elimination rate constant (k), half-life ($t_1/_2$), and intrinsic clearance (CLint) were derived from the natural log-transformed concentration vs. time data, assuming first-order kinetics.

In Vitro Transport Studies Using MDR1-Transfected MDCK Cells

MDR1-transfected MDCK cell monolayers, cultured for 5 days and obtained from the Netherlands Cancer Institute, were used for the in vitro bidirectional transport studies. Cells were maintained in Dulbecco's Modified Eagle Medium (DMEM) supplemented with 10% fetal bovine serum (FBS) and 1% penicillin-streptomycin. They were subcultured every other day at a split ratio of 1:3 to 1:5. For transport experiments, cells were seeded onto polycarbonate Transwell® filter inserts (Millipore) in 24-well plates at a density of 500,000 cells per well. After 24 hours, the medium was replaced, and the cells were cultured for an additional 4 days to allow tight junction formation before initiating the transport assays. Transport studies were performed in duplicate using a 2 μM concentration of test compound, in both apical-to-basolateral (A→B) and basolateral-to-apical (B→A) directions. The apparent permeability coefficient (P_app) was calculated using the following equation: P_{app} (cm/sec) = (Vr/C0) (1/S) (dC/dt)

Where:

- *P_app* is the apparent permeability,
- *V_r* is the volume of the receiver chamber,
- C_0 is the initial concentration in the donor chamber,
- *S* is the surface area of the cell monolayer (0.7 cm^2 for a 24-well insert),
- *dC/dt* is the rate of appearance of the compound in the receiver chamber.

Peak area ratio (PAR) was defined as the analyte peak area divided by the internal standard (IS) peak area.

The efflux ratio was calculated as: Efflux ratio $= \frac{\text{Papp B}-\text{A}}{\text{Papp A}-\text{B}}$.

Bioanalysis was carried out using LC-MS/MS. The system consisted of a Shimadzu Nexera X30 HPLC coupled with a Shimadzu LCMS-8045 Triple Quadrupole mass spectrometer.

3. Results and discussion

3.1. Chemical Synthesis

Previously, we reported the discovery of a potent and selective pyridothiophene-based α-synuclein PET imaging radioligand, [^{18}F]asyn-44. While [^{18}F]asyn-44 [16] demonstrated favorable in vitro properties and acceptable brain uptake, the presence of brain-penetrant radiometabolites in rodents will require additional characterization in higher species prior to further progression in PET imaging studies. To advance our efforts in developing CNS-penetrant and selective α-synuclein

 doi:10.20944/preprints202505.2503.v1

ligands, herein we optimized the pyridothiophene scaffold guided by central nervous system multiparameter optimization (CNS MPO) scoring and key physicochemical parameters, including molecular weight, cLogD, number of aromatic rings, and topological polar surface area (tPSA). A focused library of S,N-heterocyclic derivatives of asyn-44, with the goal of being amenable for radiolabeling, was synthesized herein through systematic modifications at the central core, left-hand side (LHS), or right-hand side (RHS) of the scaffold (Fig. 2), yielding three subclasses of compounds (as shown in the SI).

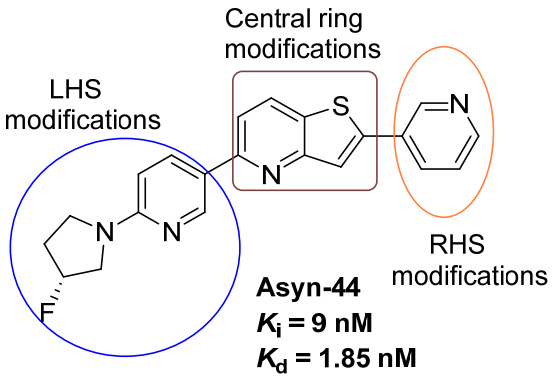

Figure 2. Design strategies for derivatization of Asyn-44.

For the synthesis of subclass I compounds (Figure 3), the pyrrolo [3,4-b]pyridin-5-one core was constructed from commercially available 6-chloro-2-methylnicotinic acid via three-step reactions [22]. This included condensation with various amine derivatives, such as 1-methyl-1H-pyrazol-3-amine, 1-methyl-1H-imidazol-4-amine, and (4-methoxyphenyl)methanamine, to afford the corresponding substituted pyrrolo [4,4-b]pyridin-5-one intermediates. These intermediates were subsequently cross-coupled with commercially available aryl boronic esters via a Suzuki–Miyaura reaction to afford the final compounds LMD-016, LMD-017, and LMD-023, as well as key intermediates used in the synthesis of LMD-064, LMD-019, and LMD-022. The non-optimized yields for these new inhibitors ranged from 1% to 60%.

To access compounds of subclass II, compound 60 was synthesized from commercially available 2,5-dibromothiophene in three steps, following a patent (WO2023133229 A2 2023-07-13) reported protocol (Supplemental). Compound **60** was subsequently derivatized into a series of analogues. Most of these derivatives were obtained via palladium-catalyzed Suzuki–Miyaura cross-coupling reactions with thiazole and aryl boronic esters, affording intermediates that served as precursors for further functionalization. These intermediates underwent Buchwald–Hartwig amination with various aryl halide derivatives to yield the final products: LMD-028, LMD-046, LMD-029, LMD-031, LMD-032, LMD-033, LMD-034, LMD-051, LMD-052, LMD-073, LMD-061, LMD-070, LMD-068, and LMD-069, with yields ranging from 0.7% to 17%. In parallel, compound **60** was subjected to hydrodebromination and subsequent deprotection, followed by Buchwald–Hartwig amination to afford LMD-031 with a yield of 1.5%. Alternatively, compound 60 underwent a palladium-catalyzed cross-coupling reaction followed by deprotection to yield 5-(1-methyl-1H-pyrazol-3-yl)-2H-thieno [3,2-c]pyrazole, which served as a key intermediate for a subsequent Buchwald–Hartwig amination. This process enabled the synthesis of a series of analogues, including LMD-054, LMD-066, LMD-067, LMD-072, LMD-074, LMD-075, LMD-076, and LMD-077, with yields ranging from 3% to 14%.

Derivatives of subclass III were obtained from both compound 3 and compound 4. Compound **3** was synthesized in two steps from commercially available thiophen-3-amine and oxalic acid. Compound **4** was prepared by bromination of compound **3**. Both compounds **3** and **4** were subsequently coupled with boronic acids or boronic acid pinacol esters under palladium catalysis to form key intermediates. These intermediates were further transformed via Suzuki–Miyaura cross-coupling and/or Buchwald–Hartwig amination to afford a series of derivatives, including LMD-001, LMD-002, LMD-009, LMD-011, LMD-049, LMD-045, LMD-005, LMD-013, LMD-060, LMD-006, LMD-

 doi:10.20944/preprints202505.2503.v1

014, LMD-062, LMD-015, LMD-024, LMD-026, LMD-036, LMD-039, LMD-040, LMD-041, LMD-063, and LMD-044, with yields ranging from 0.5% to 86%.

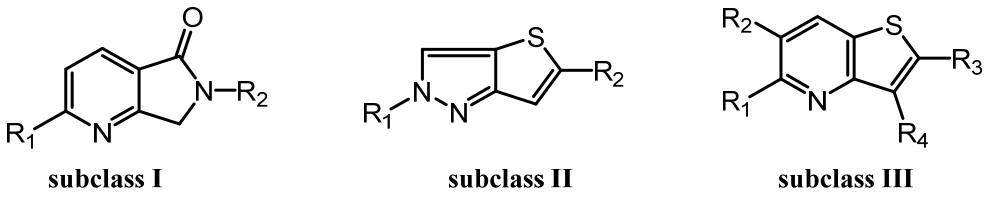

Figure 3. Three Subclasses of Novel Derivatives.

3.2. Binding Assays and SAR Studies

All screened compounds were >95% pure as determined by ^{1}H-NMR and analytical HPLC (Supporting Information). The in vitro evaluation of the synthesized derivatives was carried out to identify the most promising candidates for α-synuclein PET radiotracer development. The compounds underwent initial screening using a two-point assay, consistent with protocols described in prior work [16, 21]. This preliminary screen aimed to identify structural variants capable of displacing [^{3}H]asyn-44 in a dose-dependent manner, thereby prioritizing compounds for more detailed competition binding assays. Testing was performed in human PD brain tissue homogenates at two concentrations: 30 nM and 300 nM (Table S2.1, Supporting Information). While numerous compounds demonstrated strong displacement at the higher concentration (with <50% of [^{3}H]asyn-44 remaining bound), only a limited subset exhibited comparable activity at 30 nM. For compounds exhibiting pronounced inhibition at 300 nM (≤15% bound [^{3}H]asyn-44) and moderate to good inhibition at 30 nM (around 70% bound), full competition binding assays were conducted to determine their K_i values (Table S2.2, Supporting Information).

Among these, the SAR results are summarized in Table S2.3 of the Supporting Information. The pyrazine analogue, LMD-028, showed improved potency compared to the pyridine analogue in LMD-029. The N1 analogue in LMD-046 demonstrated greater potency than the N2 analogue in LMD-028. The piperidine ring in LMD-033 showed enhanced potency relative to the pyrrolidine analogue in LMD-051. However, replacing the pyridine ring in Asyn-44 with a pyrazine ring in LMD-033 resulted in reduced potency. Similarly, the N2 analogue in LMD-052 displayed decreased potency compared to the N1 analogue in LMD-073. Substitution of the pyrrolidine ring in LMD-052 with a piperidine ring in LMD-068 also led to a loss in potency. In a comparison between Asyn-44 and LMD-041, shifting the pyridine ring from the C-2 to the C-3 position on the central scaffold in LMD-041 resulted in diminished potency. Additionally, the pyridine ring in LMD-041 was less effective than the N-methylpyrazole ring in LMD-063. LMD-045 demonstrated improved potency due to the incorporation of a piperazine ring at the LHS, compared to LMD-041. Although both LMD-026 and LMD-027 showed reduced potency, LMD-044 exhibited improved activity, likely due to the presence of a piperazine moiety at the LHS.

Asyn-44 and the thiazole analogue LMD-006 were found to be equipotent. In contrast, the N-methylpyrazole analogue LMD-005 showed decreased potency compared to Asyn-44. The 3-methylpyrrolidine group in LMD-001 also led to reduced activity relative to the pyrrolidine analogue in LMD-002. Asyn-44 and LMD-009 displayed comparable potency, despite the presence of a pyrazine ring at the LHS in LMD-009, which did not enhance activity. The replacement of the pyridine ring at the RHS of LMD-009 with thiazole or methoxy-pyridine resulted in equipotency, while substitution with N-methylpyrazole (LMD-013) led to a loss in potency.

The piperidine analogue LMD-060 showed improved potency compared to the pyrrolidine analogue LMD-013. Substitution with a pyrazine ring at the LHS in LMD-022 and LMD-017 led to better potency than the pyridine-containing analogues LMD-064 and LMD-016. Modification of the central core in LMD-019, relative to Asyn-44, did not result in any improvement in potency. A

 doi:10.20944/preprints202505.2503.v1

significant drop in potency was observed for LMD-064 in comparison with LMD-016, LMD-019, and LMD-023.

3.3. Metabolic Stability, Permeability, and Efflux Characteristics of selected LMD Compounds

To assess metabolic stability, selected LMD compounds were incubated with human liver microsomes (h-MR), and their half-lives ($t_1/_2$) were determined (**Table 1**). The results demonstrated a broad range of metabolic stability among the compounds. LMD-022 (K_i = 16 nM) showed excellent stability with a half-life of 75 minutes. In contrast, compounds such as LMD-006 (K_i = 12 nM, $t_1/_2$ = 6.81 min), LMD-032 (K_i = 50 nM, $t_1/_2$ = 7.05 min), LMD-044 (K_i = 9.1 nM, $t_1/_2$ = 6.37 min), and LMD-051 (K_i = 6 nM, $t_1/_2$ = 7.6 min) showed rapid metabolic turnover, indicating limited stability. LMD-066 (K_i = 11.8 nM) was found to be metabolically unstable under the assay conditions. Moderate stability was observed for LMD-045 (K_i = 13.3 nM, $t_1/_2$ = 10.5 min) and LMD-051 (K_i = 9.2 nM, $t_1/_2$ = 17 min), suggesting some potential for further optimization. (Chromatograms in the Supporting Information).

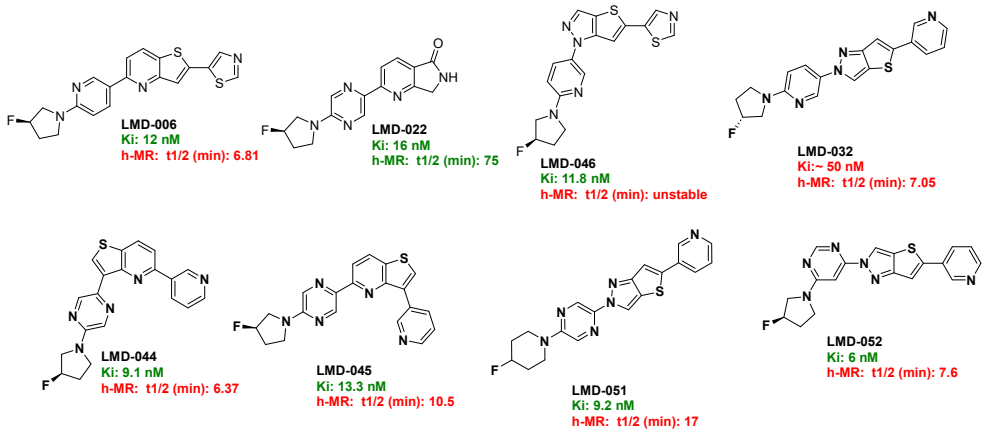

Figure 4. Active compounds.

Based on its favorable metabolic stability and binding affinity, LMD-022 was selected for further evaluation of its permeability and efflux characteristics using a bidirectional Caco-2 cell assay (**Table 2**). LMD-022 demonstrated high permeability, with an apical-to-basolateral (A→B) permeability of 40.6 × 10^{-6} cm/s and a basolateral-to-apical (B→A) permeability of 37.6 × 10^{-6} cm/s. The calculated efflux ratio was 0.93, indicating that LMD-022 is not a substrate for active efflux transporters. For comparison, digoxin, a known P-glycoprotein substrate, showed low permeability (A→B: 1.65 × 10^{-6} cm/s) and a high efflux ratio of 14.5, confirming its classification as a substrate of efflux. In contrast, propranolol, a compound with moderate permeability (A→B: 9.28 × 10^{-6} cm/s) and an efflux ratio of 0.9, was similarly categorized as not being a substrate. These results suggest that LMD-022 possesses favorable permeability characteristics and is unlikely to be limited by efflux mechanisms in vivo. (Chromatograms in the Supporting Information)

Table 1. The metabolic stability of selected LMD compounds in human liver microsomes.

Compound ID	% remaining at 5 mins	% remaining at 30 mins	$t_{1/2}$ (min)	Clint (µg/min/mg)	Clearance category[2]
LMD-032	53.3	5.02	7.05	197	High
LMD-046	3.43	NC[1]	NC	NC	NC
LMD-051	75.8	30.3	17.0	81.5	High
LMD-052	39.7	5.61	7.60	182	High
LMD-044	45.7	3.71	6.37	218	High
LMD-045	65.3	13.5	10.5	132	High
LMD-006	39.6	4.32	6.81	203	High
LMD-022	92.4	75.4	75.3	18.4	Moderate

 doi:10.20944/preprints202505.2503.v1

Verapamil	43.6	4.64	6.89	201	High

[1] NC: Not Computable. [2] As per Cyprotex Website.

Table 2. Summary of MDR1-MDCK permeability and efflux data for LMD-022 and control compounds.

Compound ID	A→B ($\times 10^{-6}$ cm/s)	B→A ($\times 10^{-6}$ cm/s)	Efflux Ratio (B→A / A→B)	Permeability Category	Efflux Category
LMD-022	40.6	37.6	0.93	High	Not a substrate
Digoxin	1.65	24	14.5	Low	Substrate of efflux
Propranolol	9.28	8.03	0.9	Medium	Not a substrate

4. Conclusions

In this study, we designed and synthesized a diverse library of 49 S,N-heterocyclic derivatives based on the pyridothiophene scaffold of the previously reported α-synuclein ligand [^{18}F]asyn-44. Through systematic structural modifications across three subclasses—thieno [3,2-b]pyridine, 6,7-dihydro-5H-pyrrolo [3,4-b]pyridin-5-one, and 2H-thieno [3,2-c]pyrazole—we identified eight compounds (LMD-006, LMD-022, LMD-029, LMD-044, LMD-045, LMD-046, LMD-051, and LMD-052) with high affinity (K_i = 6–16 nM) in PD brain tissue homogenates. Among these, LMD-022 emerged as a lead candidate, exhibiting potent binding (K_i = 16 nM), excellent metabolic stability (human liver microsome $t_{½}$ = 75 min), and favorable pharmacokinetic characteristics. Its high permeability (Caco-2 P_{app} = 40.6 × 10^{-6} cm/s) and lack of efflux liability (efflux ratio = 0.93) further support its potential as a brain-penetrant radioligand. Ongoing studies are focused on radiolabeling LMD-022 and related analogs and evaluating their in vivo performance through preclinical PET imaging.

Supplementary Materials: The supporting information can be downloaded at: The following supporting information can be downloaded at the website of this paper posted on Preprints.org.

Author Contributions: Conceptualization, N.V. and J.S.S.; methodology, C.Z. G.R.U., Y.S.M. and J.S.S.; writing—original draft preparation, C.Z.; writing—review and editing, C.Z., J.S.S. and N.V..; funding acquisition, J.S.S. and N.V. All authors have read and agreed to the published version of the manuscript.

Funding: This research was funded by The Michael J. Fox Foundation, grant number MJFF-024348, and the APC was funded by the Michael J. Fox Foundation.

Data Availability Statement: Not Applicable.

Acknowledgments: We thank Dr. Jamie Eberling (Michael J. Fox Foundation) for helpful discussions, and Manik Debnath (University of Pittsburgh, Department of Psychiatry) for technical support with the binding assays. Human PD brain tissue samples were provided by Dr. Thomas Beach (Banner/Sun Health Brain Bank, funded by the Michael J. Fox Foundation). We also thank the members of Novandi Chemistry AB and Laxai Life Sciences for chemistry and assay support.

Conflicts of Interest: C.Z. is a consultant and N.V. is a co-founder of MedChem Imaging, Inc.

Abbreviations

The following abbreviations are used in this manuscript:

PET	Positron Emission Tomography
PD	Parkinson's disease
DLB	dementia with Lewy bodies
MSA	multiple system atrophy

 doi:10.20944/preprints202505.2503.v1

References

1. Calabresi, P.; Mechelli, A.; Natale, G.; Volpicelli-Daley, L.; Di Lazzaro, G.; Ghiglieri, V., Alpha-synuclein in Parkinson's disease and other synucleinopathies: from overt neurodegeneration back to early synaptic dysfunction. *Cell Death & Disease* **2023,** 14, (3), 176.
2. Koga, S.; Sekiya, H.; Kondru, N.; Ross, O. A.; Dickson, D. W., Neuropathology and molecular diagnosis of Synucleinopathies. *Molecular Neurodegeneration* **2021,** 16, (1), 83.
3. Kuo, G.; Kumbhar, R.; Blair, W.; Dawson, V. L.; Dawson, T. M.; Mao, X., Emerging targets of α-synuclein spreading in α-synucleinopathies: a review of mechanistic pathways and interventions. *Molecular Neurodegeneration* **2025,** 20, (1), 10.
4. Tarutani, A.; Hasegawa, M., Chapter Eighteen - Prion-like propagation of α-synuclein in neurodegenerative diseases. In *Progress in Molecular Biology and Translational Science*, Teplow, D. B., Ed. Academic Press: 2019; Vol. 168, pp 323-348.
5. Radad, K.; Moldzio, R.; Krewenka, C.; Kranner, B.; Rausch, W.-D., Pathophysiology of non-motor signs in Parkinson's disease: some recent updating with brief presentation. *Exploration of Neuroprotective Therapy* **2023,** 3, (1), 24-46.
6. Kotzbauer, P. T.; Tu, Z.; Mach, R. H., Current status of the development of PET radiotracers for imaging alpha synuclein aggregates in Lewy bodies and Lewy neurites. *Clin Transl Imaging* **2017,** 5, (1), 3-14.
7. Korat, Š.; Bidesi, N. S. R.; Bonanno, F.; Di Nanni, A.; Hoàng, A. N. N.; Herfert, K.; Maurer, A.; Battisti, U. M.; Bowden, G. D.; Thonon, D.; Vugts, D.; Windhorst, A. D.; Herth, M. M., Alpha-Synuclein PET Tracer Development—An Overview about Current Efforts. *Pharmaceuticals* **2021,** 14, (9), 847.
8. Alam, M. M.; Lee, S. H.; Wasim, S.; Lee, S.-Y., PET tracer development for imaging α-synucleinopathies. *Archives of Pharmacal Research* **2025,** 48, (4), 333-350.
9. Mekala, S.; Wu, Y.; Li, Y.-M., Strategies of positron emission tomography (PET) tracer development for imaging of tau and α-synuclein in neurodegenerative disorders. *RSC Medicinal Chemistry* **2025,** 16, (2), 605-639.
10. Park, H.; Kam, T.-I.; Dawson, V. L.; Dawson, T. M., α-Synuclein pathology as a target in neurodegenerative diseases. *Nature Reviews Neurology* **2025,** 21, (1), 32-47.
11. Fernandes Gomes, B.; Farris, C. M.; Ma, Y.; Concha-Marambio, L.; Lebovitz, R.; Nellgård, B.; Dalla, K.; Constantinescu, J.; Constantinescu, R.; Gobom, J.; Andreasson, U.; Zetterberg, H.; Blennow, K., α-Synuclein seed amplification assay as a diagnostic tool for parkinsonian disorders. *Parkinsonism Relat Disord* **2023,** 117, 105807.
12. Kim, H. Y.; Chia, W. K.; Hsieh, C.-J.; Saturnino Guarino, D.; Graham, T. J. A.; Lengyel-Zhand, Z.; Schneider, M.; Tomita, C.; Lougee, M. G.; Kim, H. J.; Pagar, V. V.; Lee, H.; Hou, C.; Garcia, B. A.; Petersson, E. J.; O'Shea, J.; Kotzbauer, P. T.; Mathis, C. A.; Lee, V. M. Y.; Luk, K. C.; Mach, R. H., A Novel Brain PET Radiotracer for Imaging Alpha Synuclein Fibrils in Multiple System Atrophy. *Journal of Medicinal Chemistry* **2023,** 66, (17), 12185-12202.
13. Di Nanni, A.; Saw, R. S.; Battisti, U. M.; Bowden, G. D.; Boeckermann, A.; Bjerregaard-Andersen, K.; Pichler, B. J.; Herfert, K.; Herth, M. M.; Maurer, A., A Fluorescent Probe as a Lead Compound for a Selective α-Synuclein PET Tracer: Development of a Library of 2-Styrylbenzothiazoles and Biological Evaluation of [18F]PFSB and [18F]MFSB. *ACS Omega* **2023,** 8, (34), 31450-31467.
14. Smith, R.; Capotosti, F.; Schain, M.; Ohlsson, T.; Vokali, E.; Molette, J.; Touilloux, T.; Hliva, V.; Dimitrakopoulos, I. K.; Puschmann, A.; Jögi, J.; Svenningsson, P.; Andréasson, M.; Sandiego, C.; Russell, D. S.; Miranda-Azpiazu, P.; Halldin, C.; Stomrud, E.; Hall, S.; Bratteby, K.; Tampio L'Estrade, E.; Luthi-Carter, R.; Pfeifer, A.; Kosco-Vilbois, M.; Streffer, J.; Hansson, O., The α-synuclein PET tracer [18F] ACI-12589

 doi:10.20944/preprints202505.2503.v1

distinguishes multiple system atrophy from other neurodegenerative diseases. *Nature Communications* **2023,** 14, (1), 6750.

15. Kuebler, L.; Buss, S.; Leonov, A.; Ryazanov, S.; Schmidt, F.; Maurer, A.; Weckbecker, D.; Landau, A. M.; Lillethorup, T. P.; Bleher, D.; Saw, R. S.; Pichler, B. J.; Griesinger, C.; Giese, A.; Herfert, K., [11C]MODAG-001—towards a PET tracer targeting α-synuclein aggregates. *European Journal of Nuclear Medicine and Molecular Imaging* **2021,** 48, (6), 1759-1772.
16. Pees, A.; Tong, J.; Birudaraju, S.; Munot, Y. S.; Liang, S. H.; Saturnino Guarino, D.; Mach, R. H.; Mathis, C. A.; Vasdev, N., Development of Pyridothiophene Compounds for PET Imaging of α-Synuclein. *Chemistry* **2024,** 30, (23), e202303921.
17. Xiang, J.; Zhang, Z.; Wu, S.; Ye, K., Positron emission tomography tracers for synucleinopathies. *Molecular Neurodegeneration* **2025,** 20, (1), 1.
18. Xiang, J.; Tao, Y.; Xia, Y.; Luo, S.; Zhao, Q.; Li, B.; Zhang, X.; Sun, Y.; Xia, W.; Zhang, M.; Kang, S. S.; Ahn, E.-H.; Liu, X.; Xie, F.; Guan, Y.; Yang, J. J.; Bu, L.; Wu, S.; Wang, X.; Cao, X.; Liu, C.; Zhang, Z.; Li, D.; Ye, K., Development of an α-synuclein positron emission tomography tracer for imaging synucleinopathies. *Cell* **2023,** 186, (16), 3350-3367.e19.
19. Endo, H.; Ono, M.; Takado, Y.; Matsuoka, K.; Takahashi, M.; Tagai, K.; Kataoka, Y.; Hirata, K.; Takahata, K.; Seki, C.; Kokubo, N.; Fujinaga, M.; Mori, W.; Nagai, Y.; Mimura, K.; Kumata, K.; Kikuchi, T.; Shimozawa, A.; Mishra, S. K.; Yamaguchi, Y.; Shimizu, H.; Kakita, A.; Takuwa, H.; Shinotoh, H.; Shimada, H.; Kimura, Y.; Ichise, M.; Suhara, T.; Minamimoto, T.; Sahara, N.; Kawamura, K.; Zhang, M.-R.; Hasegawa, M.; Higuchi, M., Imaging α-synuclein pathologies in animal models and patients with Parkinson's and related diseases. *Neuron* **2024,** 112, (15), 2540-2557.e8.
20. Tian, G.-L.; Hsieh, C.-J.; Guarino, D. S.; Graham, T. J. A.; Lengyel-Zhand, Z.; Schmitz, A.; Chia, W. K.; Young, A. J.; Crosby, J.-G.; Plakas, K.; Huang, T.; Jiang, H.; Yu, Y.; Hou, C.; Lee, H.; Petersson, E. J.; Giannakoulias, S.; O'Shea, J.; Kotzbauer, P.; Tu, Z.; Mathis, C. A.; Mach, R. H., The development of a PET radiotracer for imaging alpha synuclein aggregates in Parkinson's disease. *RSC Medicinal Chemistry* **2025**.
21. Graham, T. J. A.; Lindberg, A.; Tong, J.; Stehouwer, J. S.; Vasdev, N.; Mach, R. H.; Mathis, C. A., In Silico Discovery and Subsequent Characterization of Potent 4R-Tauopathy Positron Emission Tomography Radiotracers. *J Med Chem* **2023,** 66, (15), 10628-10638.
22. Come, J. H.; Collier, P. N.; Henderson, J. A.; Pierce, A. C.; Davies, R. J.; Le Tiran, A.; O'Dowd, H.; Bandarage, U. K.; Cao, J.; Deininger, D.; Grey, R.; Krueger, E. B.; Lowe, D. B.; Liang, J.; Liao, Y.; Messersmith, D.; Nanthakumar, S.; Sizensky, E.; Wang, J.; Xu, J.; Chin, E. Y.; Damagnez, V.; Doran, J. D.; Dworakowski, W.; Griffith, J. P.; Jacobs, M. D.; Khare-Pandit, S.; Mahajan, S.; Moody, C. S.; Aronov, A. M., Design and Synthesis of a Novel Series of Orally Bioavailable, CNS-Penetrant, Isoform Selective Phosphoinositide 3-Kinase γ (PI3Kγ) Inhibitors with Potential for the Treatment of Multiple Sclerosis (MS). *Journal of Medicinal Chemistry* **2018,** 61, (12), 5245-5256.